

Superconductivity in the Ru-Doped CuIr_2Te_4 Telluride Chalcogenide

Dong Yan^a, Lingyong Zeng^a, Yishi Lin^b, Junjie Yin^c, Yuan He^a, Xing Zhang^a,
Meiling Huang^a, Meng Wang^c, Yihua Wang^b, Daoin Yao^c, Huixia Luo^{a*}

*^aSchool of Material Science and Engineering and Key Lab Polymer Composite &
Functional Materials, Sun Yat-Sen University, No. 135, Xingang Xi Road,
Guangzhou, 510275, P. R. China*

^bDepartment of Physics, Fudan University, Shanghai, 200433, China

*^cSchool of Physics, State Key Laboratory of Optoelectronic Materials and
Technologies, Sun Yat-Sen University, No. 135, Xingang Xi Road, Guangzhou,
510275, P. R. China*

**Corresponding author/authors complete details (Telephone; E-mail:) (+0086)-*

2039386124

luohx7@mail.sysu.edu.cn

Abstract

Here we report the effect of structural and superconductivity properties on Ru doped CuIr_2Te_4 telluride chalcogenide. XRD results suggest that the $\text{CuIr}_{2-x}\text{Ru}_x\text{Te}_4$ maintain the disordered trigonal structure with space group $P\bar{3}m1$ (No. 164) for $x \leq 0.3$. The lattice constants, a and c , both decrease with increasing Ru content. Temperature-dependent resistivity, magnetic susceptibility and specific-heat measurements are performed to characterize the superconducting properties systematically. Our results suggest that the optimal doping level for superconductivity in $\text{CuIr}_{2-x}\text{Ru}_x\text{Te}_4$ is $x = 0.05$, where T_c is 2.79 K with the Sommerfeld constant γ of $11.52 \text{ mJ mol}^{-1} \text{ K}^{-2}$ and the specific-heat anomaly at the superconducting transition, $\Delta C/\gamma T_c$, is approximately 1.51, which is higher than the BCS value of 1.43, indicating $\text{CuIr}_{1.95}\text{Ru}_{0.05}\text{Te}_4$ is a strongly electron-phonon coupled superconductor. The values of lower $\{H_{c1}(0)\}$ and upper $\{H_{c2}(0)\}$ critical field calculated from isothermal magnetization $\{M(H)\}$ and magneto-transport $\{\rho(T, H)\}$ measurements are 0.98 KOe and 2.47 KOe respectively, signifying that the compound is clearly a type-II superconductor. Finally, a “dome-like” shape superconducting T_c vs. x content phase diagram is established, where the charge density wave disappears at $x = 0.03$ while superconducting transition temperature (T_c) rises until it reaches its peak at $x = 0.05$, then, with decreasing when x reaches 0.3. This feature of the competition between CDW and the superconductivity could be caused by tuning the Fermi surface and density of states with Ru chemical doping.

Keywords: $\text{CuIr}_{2-x}\text{Ru}_x\text{Te}_4$; Superconductivity; Charge density wave; Quaternary telluride chalcogenide.

Introduction

The group of AB_2X_4 materials, with metallic A and B elements and X a chalcogen (O, S, Se, Te), has attracted much attention since it offers a versatile range of relevant physical properties. Generally speaking, the oxyspinels (AB_2O_4) are semiconductors with antiferromagnetic interactions, whereas the sulphospinels exhibit a much richer physical properties, such as metallic conduction, ferromagnetic, superconductivity, semiconductivity as well as antiferromagnetic interactions and so on.¹⁻⁸ Especially, the copper chalcogenide (CuB_2X_4) spinels have attracted remarkable attention due to their peculiar superconductivity and magnetism.

Copper chalcogenide $CuIr_2S_4$, for example, exhibits a temperature-induced metal-insulator (M-I) transition at 226 K, which is highly possibly attributed to the dimerization between Ir ions and the Jahn-Teller effect.⁹⁻¹³ However, the isostructural $CuIr_2Se_4$ spinel remains metallic at ambient pressure, while above 4 GPa it exhibits semi-conductive behavior in the temperature range of 7-300 K.^{9, 14} On the other hand, $CuRh_2S_4$ and $CuRh_2Se_4$ spinel are well known as superconductors with $T_c = 4.35$ K and $T_c = 3.50$ K, respectively.¹⁵⁻¹⁹ Strikingly, copper chalcogenide spinel CuV_2S_4 superconducts at 4.45-3.20 K and shows three charge density wave (CDW) states ($T_{CDW1} = 55$ K, $T_{CDW2} = 75$ K, $T_{CDW3} = 90$ K).²⁰⁻²¹

It is well known that chemical doping can efficiently tune the crystal and electronic structures of copper chalcogenide spinels, leading to the formation of novel physical properties. For example, the M-I transition was decreased with the increase of Se substitution for S at X -site of $CuIr_2S_4$ or Rh substitution for Ir at B -site of $CuIr_2S_4$.²⁴⁻²⁵ Besides, on Zn substitution for Cu in the $Cu_{1-x}Zn_xIr_2S_4$ solid solution, the M-I transition can be suppressed and superconductivity appears, with a maximum T_c of 3.4 K near $x = 0.3$.²⁷ Moreover, the superconductivity can be observed for $Cu(Ir_{1-x}Pt_x)_2Se_4$ ($0.1 \leq x \leq 0.35$) with a maximum $T_c = 1.76$ K near $x = 0.2$ with Pt substitution for Ir in the $CuIr_2Se_4$ solid solution.²⁸

Unlike CuB_2X_4 sulpho- or seleno-compounds with cubic spinel structure, CuB_2X_4 copper chalcogenide telluro-compounds tend to possess lower dimensional structure. Recently, some reports suggested that low dimensionality leads to special electronic

structures and allows relatively strong fluctuations, which may enhance superconductivity, even though charge-density wave (CDW) sometime competes, especially in the quasi-one-dimensional case.²² Intrigued by this issue, we recently have systematically studied the properties of CuIr_2Te_4 , which adopts a disordered trigonal structure with space group $P\bar{3}m1$,²³ and found coexistence of the superconducting ($T_c = 2.5$ K) and CDW ($T_{\text{CDW}} = 250$ K) in the copper telluride chalcogenide CuIr_2Te_4 .²⁴ According to our previous calculation study, we find both orbital projected band structure and density of state, the bands near the Fermi energy E_F mainly come from Te p and Ir d orbitals, similar to that of CuIr_2S_4 in spinel structure.²⁴ Therefore, it is reasonable to tune superconductivity properties by tuning the Fermi energy E_F of CuIr_2Te_4 telluride chalcogenide with chemical doping. In this article we report the synthesis and physical properties of the B -site substitution solid solution $\text{CuIr}_{2-x}\text{Ru}_x\text{Te}_4$ ($0.0 \leq x \leq 0.3$). The structural properties of the AB_2X_4 -type telluro-compounds $\text{CuIr}_{2-x}\text{Ru}_x\text{Te}_4$ ($0.0 \leq x \leq 0.3$) was characterized via X-ray diffraction (XRD). We characterize the effect of Ru substitution on the superconducting transition through temperature-dependent resistivity, magnetic susceptibility and specific-heat measurements. All measurements consistently confirm that the optimal doping level for superconductivity in $\text{CuIr}_{2-x}\text{Ru}_x\text{Te}_4$ is $x = 0.05$. The specific-heat anomaly at the superconducting transition, $\Delta C/\gamma T_c$, is approximately 1.51, which indicates that $\text{CuIr}_{1.95}\text{Ru}_{0.05}\text{Te}_4$ is a strong electron-phonon coupling BCS type superconductor. A “dome-like” shape electronic phase diagram between charge density wave (CDW) and superconducting transition temperature T_c versus Ru doping content x has been established experimentally for this system. The CDW was immediately suppressed even with small amount Ru doping at $x = 0.03$ while the superconducting transition temperature (T_c) rises until it reaches its peak at $x = 0.05$, then, with decreasing when x reaches 0.3. With discovery of this doping superconductor of CuIr_2Te_4 , we found the effective method to improve the T_c and also provides guidance for us to study other doping systems. This feature of the competition between CDW and the superconductivity could be induced by tuning the Fermi surface and density of states with Ru chemical doping.

Experimental Section

Polycrystalline samples of $\text{CuIr}_{2-x}\text{Ru}_x\text{Te}_4$ ($0.0 \leq x \leq 0.30$) were synthesized in two steps by a solid-state reaction method. First, the mixture of high-purity, cleaned fine powders of Cu (99.9 %), Ir (99.9 %), Ru (99.999 %) and Te (99.999 %) in the appropriate stoichiometric ratios were heated in sealed evacuated silica glass tubes at a rate of 1 °C/min to 850 °C and held there for 96 hours. Subsequently, the as-prepared powders were reground, re-pelletized, and sintered again, by heating at a rate of 3 °C/min to 850 °C and holding there for 72 hours. The identity and phase purity of the samples were determined by powder X-ray diffraction (PXRD) using a Bruker D8 Advance ECO with Cu $K\alpha$ radiation and a LYNXEYE-XE detector. To determine the unit cell parameters, profile fits were performed on the powder diffraction data in the FULLPROF diffraction suite using Thompson-Cox-Hastings pseudo-Voigt peak shapes.²⁹ Measurements of the temperature dependent electrical resistivity (4-point method), specific heat, and magnetic susceptibility of the materials were performed in a DynaCool Quantum Design Physical Property Measurement System (PPMS). There was no indication of air-sensitivity of the materials during the study. T_c s determined from susceptibility data were estimated conservatively: T_c was taken as the intersection of the extrapolations of the steepest slope of the susceptibility in the superconducting transition region and the normal state susceptibility; for resistivities, the midpoint of the resistivity $\rho(T)$ transitions was taken, and, for the specific heat data, the critical temperatures obtained from the equal area construction method were employed.

Results and Discussion

Fig. 1 show the powder X-ray diffraction patterns at room temperature and fitting unit cell parameters for $\text{CuIr}_{2-x}\text{Ru}_x\text{Te}_4$ ($0.0 \leq x \leq 0.30$). XRD results indicates that the solubility limit for Ru substitution in CuIr_2Te_4 is $x = 0.30$. With higher Ru contents, the cubic RuTe_2 phase is obviously found as an impurity. **Fig. 1a** shows the detail refinement results of the selected $\text{CuIr}_{1.95}\text{Ru}_{0.05}\text{Te}_4$ powder. Most of the reflections can be indexed in the $P\bar{3}m1$ space group and the tiny impurity is attributed to the unreacted Ir. The lattice parameters are obtained to be $a = 3.9360$ (3) Å and $c = 5.3917$ (5) Å. The

inset pattern shows that $\text{CuIr}_{2-x}\text{Ru}_x\text{Te}_4$ adopts a disordered trigonal structure, which embodies a two-dimensional (2D) IrTe_2 layers and intercalated by Cu between the layers, with Ir partial replacing by Ru. We determined the unit cell parameters by fitting the powder X-ray diffraction data, which were shown at **Fig. 1b**. With the increasing Ru contents, unit cell parameters a and c decreased linearly. Cell parameters a decreased from 3.9397(5) Å ($x = 0$) to 3.9238 (2) Å ($x = 0.30$), meanwhile, parameters c decreased from 5.3965 (3) Å ($x = 0$) to 5.3776 (6) Å ($x = 0.30$). The enlargement of (001) peak in **Fig. 1c** shows obvious right shift with the increasing contents of Ru. This phenomenon was also according with the decline of fitting unit cell parameters c in **Fig. 1b** by the means of crystal plane spacing formula.

We next perform the temperature dependence of the electrical resistivity $\rho(T)$ and magnetic susceptibility $M(T)$ measurements for $\text{CuIr}_{2-x}\text{Ru}_x\text{Te}_4$ ($0.0 \leq x \leq 0.30$). **Fig. 2a** show the temperature dependence of the normalized electrical resistivities ($\rho/\rho_{300\text{K}}$) for the polycrystalline samples of $\text{CuIr}_{2-x}\text{Ru}_x\text{Te}_4$ ($0.0 \leq x \leq 0.30$). At low temperatures (see **Fig. 2b**), a clear, sharp drop of $\rho(T)$ is observed in the $\text{CuIr}_{2-x}\text{Ru}_x\text{Te}_4$ samples ($0.0 \leq x \leq 0.20$) except for the highest doping content sample $\text{CuIr}_{1.7}\text{Ru}_{0.3}\text{Te}_4$, signifying the onset of superconductivity at low temperatures. The transition temperature (T_c) slightly rises until it reaches its peak at $x = 0.05$, then, disappears when x reaches 0.3. This trend is also clearly seen in the susceptibility data (**Fig. 2c**) - the onset of the negative magnetic susceptibility signaling the systematical superconducting state present a “dome” shape shifts with increasing x value for $\text{CuIr}_{2-x}\text{Ru}_x\text{Te}_4$. The superconducting volume fraction can be estimated approximately to be 96 %, which reveals the high purity of the $\text{CuIr}_{2-x}\text{Ru}_x\text{Te}_4$ ($0.0 \leq x \leq 0.20$) samples. In addition, it is obviously seen that there are all no CDW humps for the Ru-doped compounds $\text{CuIr}_{2-x}\text{Ru}_x\text{Te}_4$ ($0.03 \leq x \leq 0.30$) in the temperature-dependent resistivity results, indicating that the CDW state can be suppressed even by small amount substitution Ru for Ir in the host compound CuIr_2Te_4 , as shown in the **Fig. 2a**. To further prove it, we adopt the measurement of the magnetic susceptibility at applied field of 1T for the smallest doping content compound $\text{CuIr}_{1.97}\text{Ru}_{0.03}\text{Te}_4$. As shown in **Fig. 2d**, unlike the pristine sample CuIr_2Te_4 , the susceptibility exhibits no change around 250 K, which consistently indicate the CDW

transition has been suppressed completely with small amount Ru doping at $x = 0.03$. This significant feature of the interplay between CDW and the superconductivity could be attributed to modifying the Fermi surface and density of states with Ru chemical doping.

Temperature-dependent measurements of the magnetization under incremental magnetic field $M(H)$ were applied to determine the upper critical field $\mu_0 H_{c1}(0)$. We choose the optimal doping superconductor to test. **Fig. 3** shows how the $\mu_0 H_{c1}(0)$ for the optimal $\text{CuIr}_{1.95}\text{Ru}_{0.05}\text{Te}_4$ compound was determined. First, applied field magnetization measurements $M(H)$ were performed at 1.8, 2.0, 2.2 K and 2.4 K to calculate the demagnetization factor (N). With the hypothesis that the beginning linear response to the magnetic field is perfectly diamagnetic ($dM/dH = -1/4\pi$) for this bulk superconductor, we obtained the values of demagnetization factor N , of 0.55 – 0.75 (from $N = 1/4\pi\chi_V + 1$), where $\chi_V = dM/dH$ is the value of linearly fitted slope for the bottom left corner inset of **Fig. 3**. The experimental data can be fitted with the formula $M_{\text{fit}} = a + bH$ at low magnetic fields, where a is an intercept and b is a slope from fitting the low magnetic field magnetization measurements data. The up-right corner inset of **Fig. 3** shows the $M(H) - M_{\text{fit}}$ data versus the magnetic field(H). $\mu_0 H_{c1}^*$ was determined at the field when M deviates by $\sim 1\%$ above the fitted data (M_{fit}), as is the common practice.³⁰ We can calculate the lower critical field $\mu_0 H_{c1}(T)$ in the consideration of the demagnetization factor (N), *via* using the relation $\mu_0 H_{c1}(T) = \mu_0 H_{c1}^*(T) / (1 - N)$.³¹⁻³³ The main panel of **Fig. 3** reveals the $\mu_0 H_{c1}(T)$ as the function of temperature for $\text{CuIr}_{1.95}\text{Ru}_{0.05}\text{Te}_4$. We estimated the $\mu_0 H_{c1}(0)$ by fitting the $\mu_0 H_{c1}(T)$ data *via* the formula $\mu_0 H_{c1}(T) = \mu_0 H_{c1}(0) [1 - (T/T_c)^2]$, which was shown by the black solid lines. The obtained zero-temperature lower critical field $\mu_0 H_{c1}(0)$ for $\text{CuIr}_{1.95}\text{Ru}_{0.05}\text{Te}_4$ was 0.098 T (**Table 1**), which is higher than that of the host compound CuIr_2Te_4 .

With the purpose of estimating the critical field $\mu_0 H_{c2}(0)$, we examined temperature dependent electrical resistivity at various applied fields $\rho(T, H)$ for $\text{CuIr}_{1.95}\text{Ru}_{0.05}\text{Te}_4$ sample. **Fig. 4** exhibits the $\rho(T, H)$ measurement data for $\text{CuIr}_{1.95}\text{Ru}_{0.05}\text{Te}_4$. **Inset of Fig. 4** shows upper critical field values $\mu_0 H_{c2}$ plotted *vs* temperature with T_c s obtained from

resistivity at different applied fields. The $\mu_0 H_{c2}$ vs T curve near T_c of $\text{CuIr}_{1.95}\text{Ru}_{0.05}\text{Te}_4$ sample shows the well linearly fitting, which is represented by solid line. The value of fitting data slope (dH_{c2}/dT) of $\text{CuIr}_{1.95}\text{Ru}_{0.05}\text{Te}_4$ sample was shown in **Table 1**. We can estimate the zero-temperature upper critical field ($\mu_0 H_{c2}(T)$) of 0.247 T for $\text{CuIr}_{1.95}\text{Ru}_{0.05}\text{Te}_4$ from the data, using the Werthamer-Helfand-Hohenberg (WHH) expression formula $\mu_0 H_{c2}(T) = -0.693 T_c (dH_{c2}/dT_c)$ for the dirty limit superconductivity.³³⁻³⁷ The obtained $\mu_0 H_{c2}(T)$ for $\text{CuIr}_{1.95}\text{Ru}_{0.05}\text{Te}_4$ is two times higher than that of the pristine CuIr_2Te_4 , as summarized in **Table 1**. In addition, the Pauli limiting field ($\mu_0 H^P(T)$) of $\text{CuIr}_{1.95}\text{Ru}_{0.05}\text{Te}_4$ can be calculated from $\mu_0 H^P(T) = 1.86 T_c$. The calculated values of $\mu_0 H^P(T)$ was also larger than that of the host compound CuIr_2Te_4 . Then, with this formula $\mu_0 H_{c2}(T) = \frac{\phi_0}{2\pi\xi_{\text{GL}}^2}$, where ϕ_0 is the flux quantum, the Ginzburg-Laudau coherence length ($\xi_{\text{GL}}(0)$) was calculated ~ 36.3 nm for $\text{CuIr}_{1.95}\text{Ru}_{0.05}\text{Te}_4$ (**Table 1**).

Temperature-dependent specific-heat measurements were performed with the exception of magnetic susceptibility and resistivity measurements to confirm that superconductivity is an intrinsic property of $\text{CuIr}_{1.95}\text{Ru}_{0.05}\text{Te}_4$. **Fig. 5** (main panel) plots C_p/T vs T^2 in zero and 3 tesla applied field in temperature range of 2 - 10 K. The relationship for the C_p/T vs T in zero applied field near the transition temperature was further plotted in the inset of **Fig 5**. As it can be seen, there is large anomaly hump in the specific heat data, which agrees with bulk superconductivity in $\text{CuIr}_{1.95}\text{Ru}_{0.05}\text{Te}_4$. The superconducting transition temperature (T_c) can be confirmed by equal-entropy constructions of the idealized specific-heat capacity jump (shown with purple shading). The T_c of $\text{CuIr}_{1.95}\text{Ru}_{0.05}\text{Te}_4$ was determined to be 2.72 K, which is very close to the T_c s obtained from the resistivity and magnetic susceptibility measurements. Further, we got the values of γ and β (**Fig. 5**) from fitting the data got under 3 tesla applied field in temperature range of 2 - 10 K. The normalized specific heat jump value $\Delta C/\gamma T_c$ obtained from the data (**inset of Fig. 5**) was 1.51 for $\text{CuIr}_{1.95}\text{Ru}_{0.05}\text{Te}_4$, which is higher than the Bardeen-Cooper-Schrieffer (BCS) weak-coupling limit value (1.43), confirming bulk superconductivity. Then we obtain the Debye temperature by the formula $\Theta_D =$

$(12\pi^4 nR/5\beta)^{1/3}$ by using the fitted value of β , where n is the number of atoms per formula unit and R is the gas constant. Thus, we can estimate the electron-phonon coupling constant (λ_{ep}) by using the Debye temperature (Θ_D) and critical temperature T_c from the

inverted McMillan formula: $\lambda_{ep} = \frac{1.04 + \mu^* \ln\left(\frac{\Theta_D}{1.45T_c}\right)}{(1 - 1.62\mu^*) \ln\left(\frac{\Theta_D}{1.45T_c}\right) - 1.04}$ ³³. This resultant λ_{ep} is 0.67,

suggesting that $\text{CuIr}_{1.95}\text{Ru}_{0.05}\text{Te}_4$ belongs to a strongly electron-phonon coupled superconductor. The electron density of states at the Fermi level ($N(E_F)$) can be calculated from $N(E_F) = \frac{3}{\pi^2 k_B^2 (1 + \lambda_{ep})} \gamma$ with the γ and λ_{ep} . We got the value that $N(E_F) = 2.92$ states/eV f.u. for $\text{CuIr}_{1.95}\text{Ru}_{0.05}\text{Te}_4$ and $N(E_F) = 2.72$ states/eV f.u. for CuIr_2Te_4 (**Table 1**). This result indicates that the higher density of electronic states at the Fermi energy matched the higher transition temperature due to the Ru doping into CuIr_2Te_4 .

To further understand the effect of doping on superconducting transition temperature, we have established the electronic phase diagram plotted T_c s vs x doping content for $\text{CuIr}_{2-x}\text{Ru}_x\text{Te}_4$ ($0.0 \leq x \leq 0.30$), as shown in **Fig. 6**. All the T_c s were obtained from the temperature dependence of the normalized ($\rho/\rho_{300\text{K}}$) resistivities and magnetic susceptibility data. From the phase diagram we can easily find that the T_c vs. x content present a “dome-like” shape. Using Ru chemical doping as finely controlled tuning parameters, the CDW state has been mediately surprised, meanwhile superconducting transition temperature (T_c) rises to the first peak ($x = 0.05$) and then decreases until it reaches its minimum value at $x = 0.3$. Nevertheless, the reason why the CDW state can be suppressed by Ru doping so quickly has not yet been studied. Through systematic research the doping system of CuIr_2Te_4 , we found that materials’ electronic structure can be effected by the doping content consequently affect their physical properties like superconducting transition temperature, also there is large room for further exploration the interplay of CDW and superconductivity in AB_2X_4 system.

Conclusion

Here the solid solutions $\text{CuIr}_{2-x}\text{Ru}_x\text{Te}_4$ ($0.0 \leq x \leq 0.3$) have been successfully synthesized *via* solid-state reaction to study the effect of the B -site substitution on the

superconductivity. The structural and superconductivity properties for this system was evaluated systematically by means of powder x-ray diffraction (XRD), magnetization, resistivity and specific-heat measurements. XRD analysis reveals that $\text{CuIr}_{2-x}\text{Ru}_x\text{Te}_4$ ($0.0 \leq x \leq 0.3$) crystallized a disordered trigonal structure with space group $P\bar{3}m1$ (No. 164). Specific-heat, isothermal magnetization $\{M(H)\}$ and magneto-transport $\{\rho(T, H)\}$ measurements results signify that the optimal doping content compound $\text{CuIr}_{1.95}\text{Ru}_{0.05}\text{Te}_4$ is a strongly electron-phonon coupled type-II superconductor with $T_c \approx 2.79(1)$ K, a lower critical field $H_{c1}(0) = 980$ Oe and an upper critical field, $H_{c2}(0) = 2470$ Oe. Finally, we have established a “dome-like” shape electronic phase diagram, in which CDW-superconducting transition temperature as a function of Ru doping content x . We can easily find that the CDW has been suppressed immediately at $x = 0.03$ and the superconducting transition temperature (T_c) rises to the first peak ($x = 0.05$) and then decreases until it reaches its minimum value at $x = 0.3$, which displays a good material platform for further study the competition between CDW and superconductivity.

Acknowledgment

The authors thank T. Klimczuk, B. Shen and T. R. Chang for valuable discussions. H. X. Luo acknowledges the financial support by Natural Science Foundation of China (No. 21701197 and No. 11922415). D. X. Yao are supported by NKRDPC Grants No. 2017YFA0206203, No. 2018YFA0306001, NSFC-11574404, and Leading Talent Program of Guangdong Special Projects.

Reference:

- [1] T. J. Coutts, D. L. Young, X. Li, W. P. Mulligan, and X. Wu, *J. Vac. Sci. Technol.* **A18**, 2646 (2000).
- [2] M. Dekkers, G. Rijnders, and D. H. A. Blank, *Appl. Phys. Lett.* **90**, 021903 (2007).
- [3] C. A. Hoel, T. O. Mason, J.-F. Gaillard, and K. R. Poeppelmeier, *Chem. Mater.* **22**, 3569 (2010).
- [4] F. K. Lotgering, *Philips Res. Rep.*, **11**, 190 (1956).
- [5] S. Nagata, T. Hagino, Y. Seki, and T. Bitoh, *Phys. B*, **194-196**, 1077 (1994).

- [6] P. G. Radaelli, Y. Horibe, M. J. Gutmann, H. Ishibashi, C. H. Chen, R. M. Ibberson, Y. Koyama, Y. S. Hor, V. Kiryukhin, and S. W. Cheong, *Nature*, **416**, 155 (2002).
- [7] T. Hagino, Y. Seki, N. Wada, S. Tsuji, T. Shirane, K. I. Kumagai, and S. Nagata, *Phys. Rev. B*, **51**, 12673 (1995).
- [8] M. Ito, A. Taira, and K. Sonoda, *Acta Physica Polonica A.*, **131**, 6 (2017).
- [9] T. Hagino, Y. Seki, and S. Nagata, *Phys. C*, **235–240**, 1303(1994).
- [10] T. Furubayashi, T. Matsumoto, T. Hagino, and S. Nagata, *J. Phys. Soc. Jpn.*, **63**, 3333 (1994).
- [11] T. Hagino, T. Tojo, T. Atake, and S. Nagata, *Philos. Mag.* **B71**, 881 (1995).
- [12] T. Oda, M. Shirai, N. Suzuki, and K. Motizuki, *J. Phys.: Condens. Matter*, **7**, 4433 (1995).
- [13] G. Oomi, T. Kagayama, I. Yoshida, T. Hagino, and S. Nagata, *J. Magn. Magn. Mater.*, **140–144**, 157 (1995).
- [14] T. Furubayashi, T. Kosaka, J. Tang, T. Matsumoto, Y. Kato, and S. Nagata, *J. Phys. Soc. Jpn.*, **66** 1563(1997).
- [15] M. Robbins, R. H. Willens, and R. C. Miller, *Solid State Commun.*, **5**, 933 (1967).
- [16] F. K. Lotgering, and R. P. Van Stapele, *J. Appl. Phys.*, **39**, 417 (1968).
- [17] F. K. Lotgering, *J. Phys. Chem. Solids*, **30**, 1429 (1969).
- [18] F. J. DiSalvo and J. V. Waszczak, *Phys. Rev. B*, **26**, 2501 (1982).
- [19] R. N. Shelton, D. C. Johnston, and H. Adrian, *Solid State Commun.*, **20**, 1077 (1976).
- [20] R. M. Fleming, F. J. DiSalvo, R. J. Cava and J. V. Waszczak, *Phys. Rev. B*, **24**, 2850 (1981).
- [21] N. L. Nagard, A. Katty, G. Collin, O. Gorochoy, and A. Willig, *J. Solid State Chem.*, **27**, 267 (1979).
- [22] S. V. Smaalen, *Acta Crystallogr.* **A61**, 51 (2005).
- [23] S. Nagata, N. Kijima, S. Ikeda, N. Matsumoto, R. Endoh, S. Chikazawa, I. Shimono, and H. Nishihara, *J. Phys. Chem. Solids*, **60**, 163 (1999).
- [24] D. Yan, Y. J. Zeng, G. H. Wang, Y. Y. Liu, J. J. Yin, T.-R. Chang, H. Lin, M. Wang, J. Ma, S. Jia, D.-X. Yao, H. X. Luo, *arXiv:1908.05438* (2019).
- [25] S. Nagata, N. Matsumoto, Y. Kato, T. Furubayashi, T. Matsumoto, J. P. Sanchez, and P. Vulliet, *Phys. Rev. B*, **58**, 6844 (1998).
- [26] N. Matsumoto, R. Endoh, S. Nagata, T. Furubayashi, and T. Matsumoto, *Phys. Rev. B*, **60**, 5258 (1999).
- [27] H. Suzuki, T. Furubayashi, G. Cao, H. Kitazawa, A. Kamimura, K. Hirata and T. Matsumoto, *J. Phys. Soc. Jpn.*, **68**, 2495 (1999).
- [28] H. X. Luo, T. Klimczuk, L. MÜchler, L. Schoop, D. Hirai, M. K. Fuccillo, C. Felser, and R. J. Cava, *Phys. Rev. B*, **87**, 214510 (2013).
- [29] J. Rodríguez-Carvajal, *Comm. Powder Diffr.*, **26**, 12 (2001).
- [30] H. X. Luo, W. W. Xie, J. Tao, I. Pletikosic, T. G. Valla, S. Sahasrabudhe, G. Osterhoudt, E. Sutton, K. S. Burch, E. M. Seibel, J. W. Krizan, Y. M. Zhu, and R. J. Cava, *Chem. Mater.*, **28**, 1927 (2016).
- [31] M. J. Winiarski, B. Wiendlocha, S. Gołąb, S. K. Kushwaha, P. Wiśniewsk, D. Kaczorowski, J. D. Thompson, R. J. Cava, and T. Klimczuk, *Phys. Chem. Chem. Phys.*,

18, 21737 (2016).

[32] C. S. Yadav, and P. L. Paulose, *New J. Phys.*, **11**, 103046 (2009).

[33] W. L. McMillan, *Phys. Rev.*, **167**, 331(1968).

[34] J. A. Wilson, A. S. Barker, F. J. Di Salvo, and J. A. Ditzenberger, *Phys. Rev. B*, **18**, 2866 (1978).

[35] W. Kohn, *Phys. Rev. Lett.*, **19**, 439 (1967).

[36] N. R. Werthamer, E. Helfand, and P. C. Hohenberg, *Phys. Rev.*, **147**, 415 (1967).

[37] V. Z. Kresin, and S. A. Wolf, *Plenum Press, New York and London*, 150 (1990).

Table 1. Comparison of superconducting parameters in AB_2X_4 superconductors

Material	CuIr _{1.95} Ru _{0.05} Te ₄	CuIr ₂ Te ₄	CuRh ₂ S ₄	CuRh ₂ Se ₄	Cu _{0.7} Zn _{0.3} Ir ₂ S ₄	CuIr _{1.6} Pt _{0.4} Se ₄
T_c (K)	2.79	2.50	4.7	3.5	3.4	1.76
γ (mJ mol ⁻¹ K ⁻²)	11.52	10.57	26.9	21.4		16.5
β (mJ mol ⁻¹ K ⁻⁴)	2.54	2.15				1.41
Θ_D (K)	174.8(1)	185.5 (2)	258	218		212
$\Delta C/\gamma T_c$	1.51	1.82	1.89	1.68		1.58
λ_{ep}	0.67	0.65	0.66	0.63		0.57
$N(E_F)$ (states/eV f.u)	2.92	2.72				4.45
$-dH_{c2}/dT$ (T/K)	0.125	0.066	0.614	0.181		2.62
$\mu_0 H_{c2}(T)$	0.247	0.12	2.0	0.44		3.2
$\mu_0 H^P(T)$	5.24	4.65	8.74	6.51	6.32	3.27
$\mu_0 H_{c1}(T)$	0.098	0.028				
$\xi_{GL}(0)$ (nm)	36.3	52.8			-	0.96

Table 2. Rietveld refinement structural parameters of CuIr_{1.95}Ru_{0.05}Te₄. Space group $P-3m1$ (No. 164), $a = b = 3.9360(1)$ Å and $c = 5.3917(2)$ Å, $R_p = 6.29$ %, and $R_{wp} = 9.90$ %.

Label	x	y	z	Site	OCC.
Ir	0.00000	0.00000	0.00000	1a	0.950
Ru	0.00000	0.00000	0.00000	1a	0.050
Te	0.33330	0.66670	0.2308(4)	2d	1.000
Cu	0.00000	0.00000	0.50000	1b	0.500

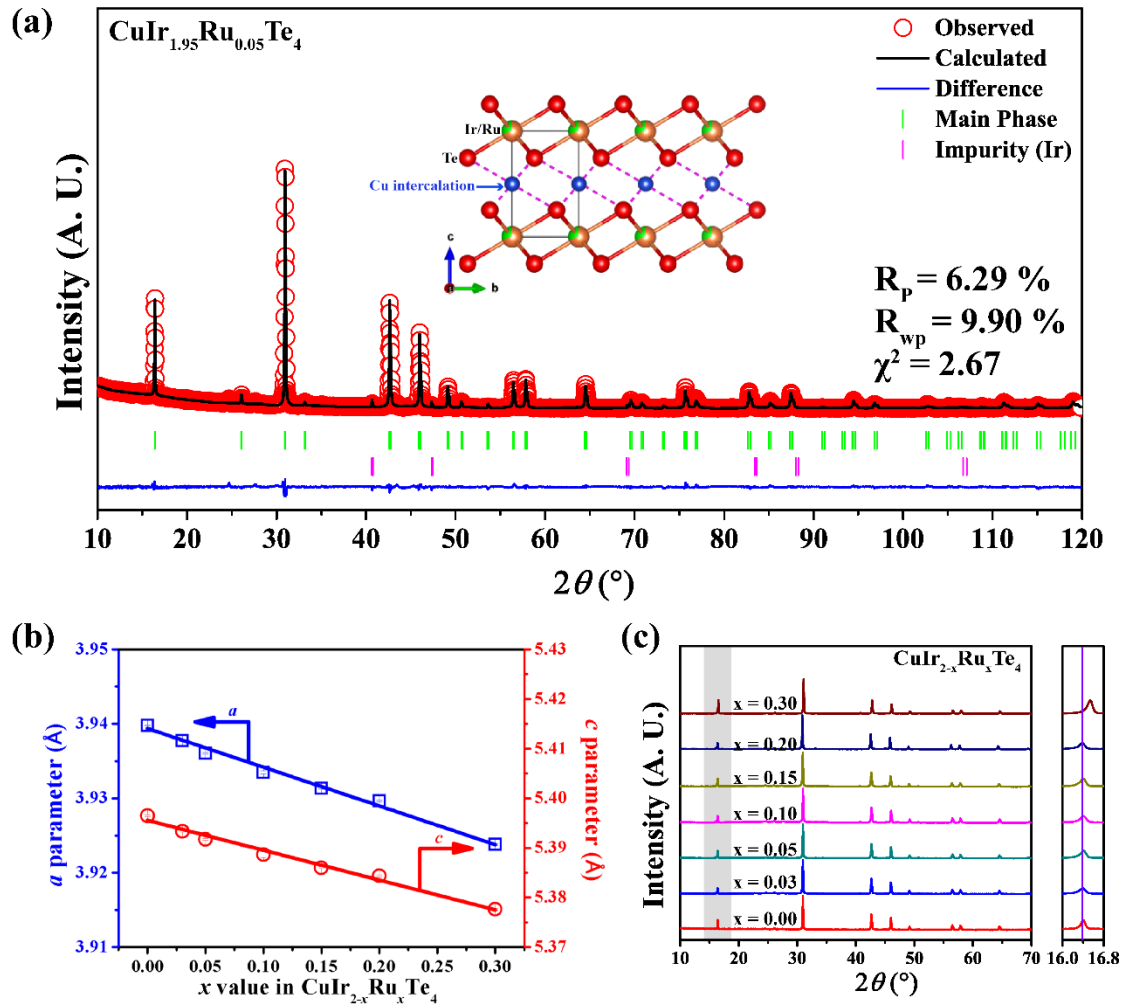


Figure 1. Structural and chemical characterization of $\text{CuIr}_{2-x}\text{Ru}_x\text{Te}_4$. (A) Powder XRD patterns (Cu $K\alpha$) for the $\text{CuIr}_{2-x}\text{Ru}_x\text{Te}_4$ samples studied ($0.0 \leq x \leq 0.30$). Inset shows the enlargement of peak (001). (B) The evolution of lattice parameter a and c of $\text{CuIr}_{2-x}\text{Ru}_x\text{Te}_4$. (C) Powder XRD pattern with Rietveld refinement for $\text{CuIr}_{1.95}\text{Ru}_{0.05}\text{Te}_4$.

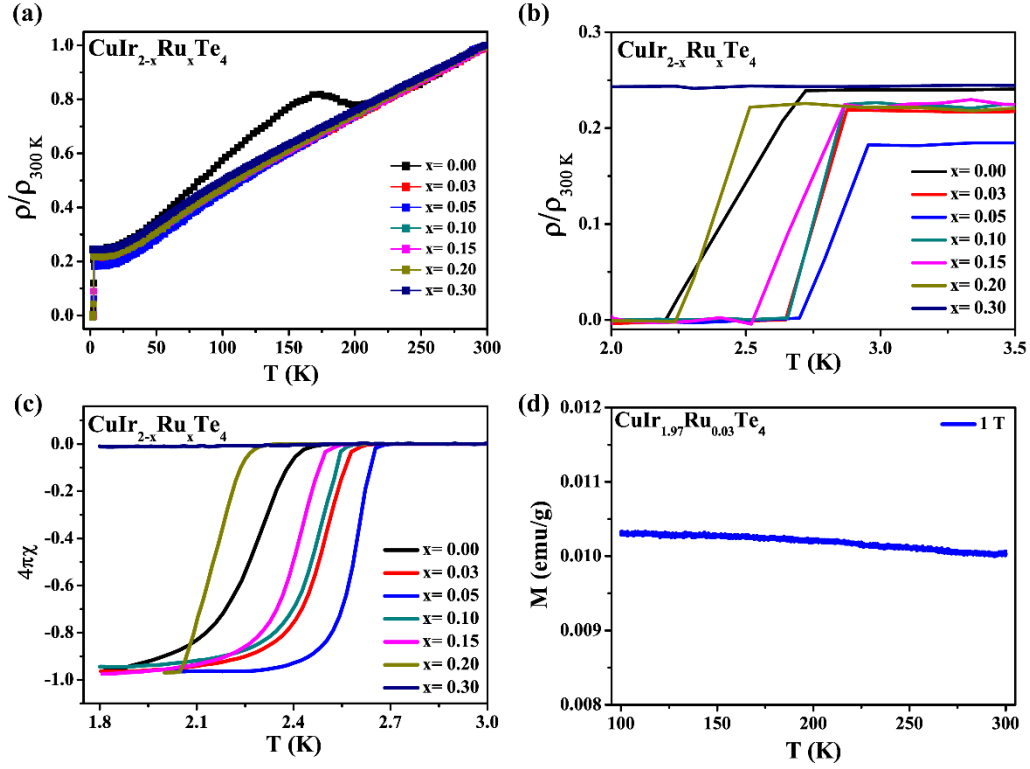


Figure 2. Transport characterization of the normal states and superconducting transitions for $\text{CuIr}_{2-x}\text{Ru}_x\text{Te}_4$. (a) The temperature dependence of the resistivity ratio ($\rho/\rho_{300\text{K}}$) for polycrystalline $\text{CuIr}_{2-x}\text{Ru}_x\text{Te}_4$ ($0.0 \leq x \leq 0.30$). (b) The temperature dependence of the resistivity ratio ($\rho/\rho_{300\text{K}}$) for polycrystalline $\text{CuIr}_{2-x}\text{Ru}_x\text{Te}_4$ at low temperature. (c) Magnetic susceptibilities for $\text{CuIr}_{2-x}\text{Ru}_x\text{Te}_4$ ($0.0 \leq x \leq 0.30$) at the superconducting transitions; applied DC fields are 20 Oe. (d) Magnetic susceptibility of $\text{CuIr}_{1.97}\text{Ru}_{0.03}\text{Te}_4$ as a function of temperature at applied field of 1 tesla.

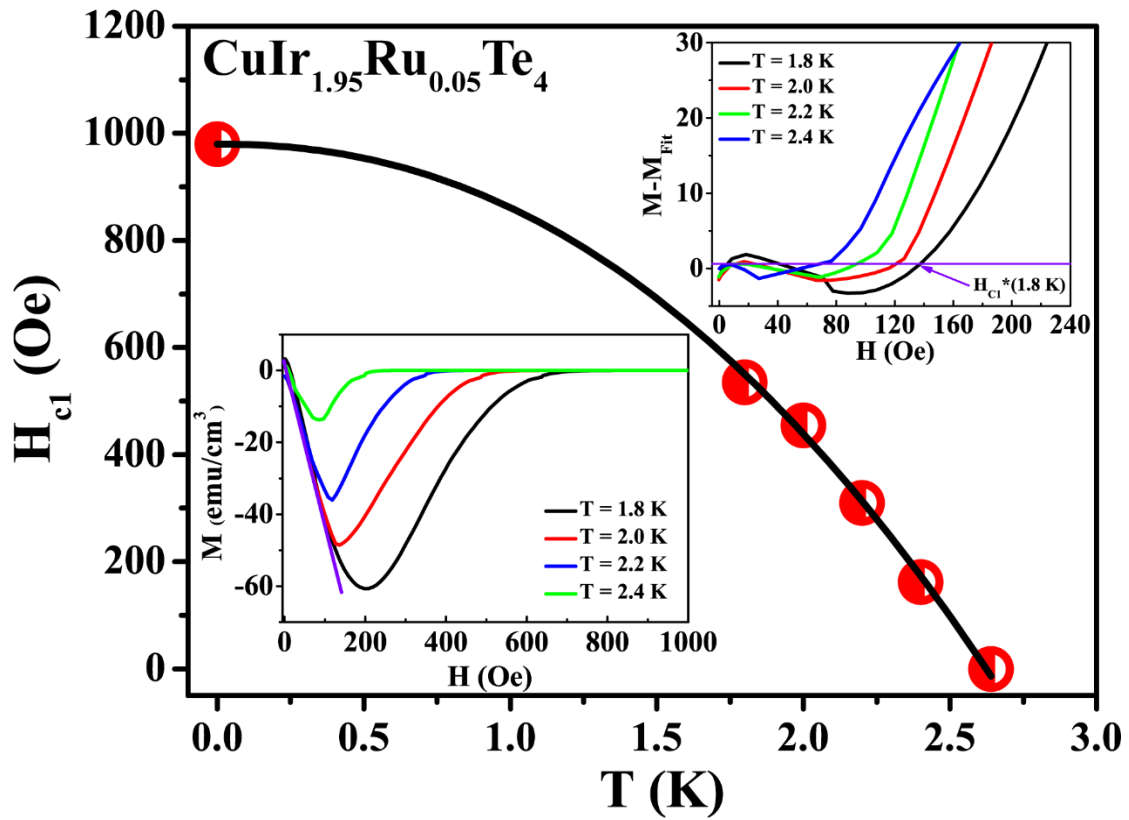


Figure 3. Temperature dependence of the lower critical field ($\mu_0 H_{c1}$) for CuIr_2Te_4 . Bottom left corner inset shows magnetic susceptibility at low applied magnetic fields at various temperatures for $\text{CuIr}_{1.95}\text{Ru}_{0.05}\text{Te}_4$. Up right inset shows $M - M_{\text{fit}}$ vs H .

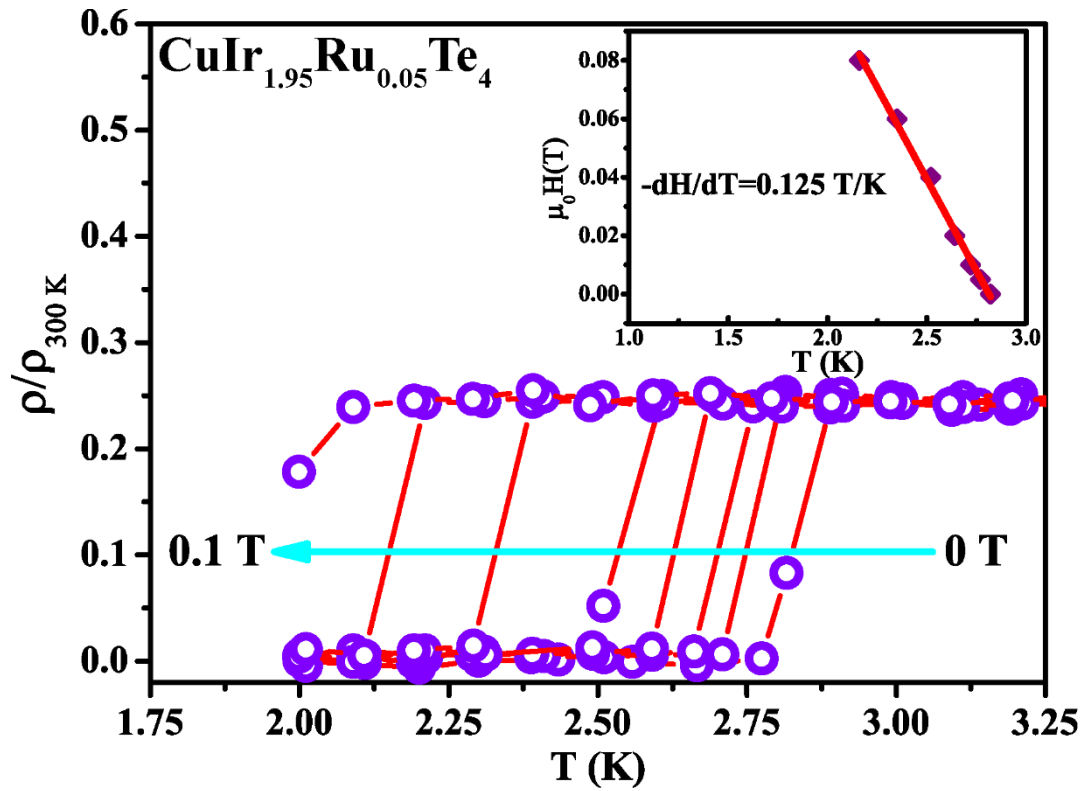


Figure 4. Low temperature resistivity at various applied fields for $\text{CuIr}_{1.95}\text{Ru}_{0.05}\text{Te}_4$. Inset shows $\mu_0 H(T)$ at different T_c s, red solid line shows linearly fitting to the data to estimate $\mu_0 H_{c2}$.

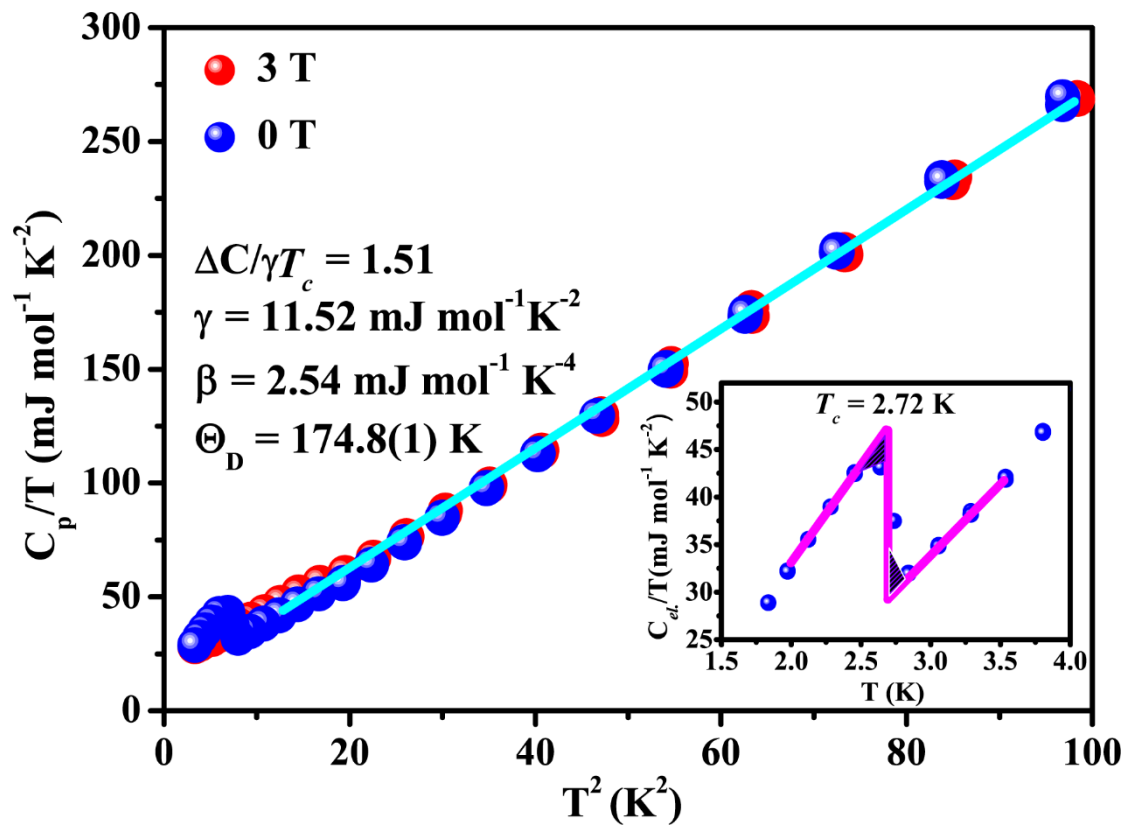


Figure 5. Heat capacity characterization of $\text{CuIr}_{1.95}\text{Ru}_{0.05}\text{Te}_4$. Debye temperature of $\text{CuIr}_{1.95}\text{Ru}_{0.05}\text{Te}_4$ obtained from fits to data in applied field. Inset shows the heat capacity through the superconducting transition without applied magnetic field for $\text{CuIr}_{1.95}\text{Ru}_{0.05}\text{Te}_4$.

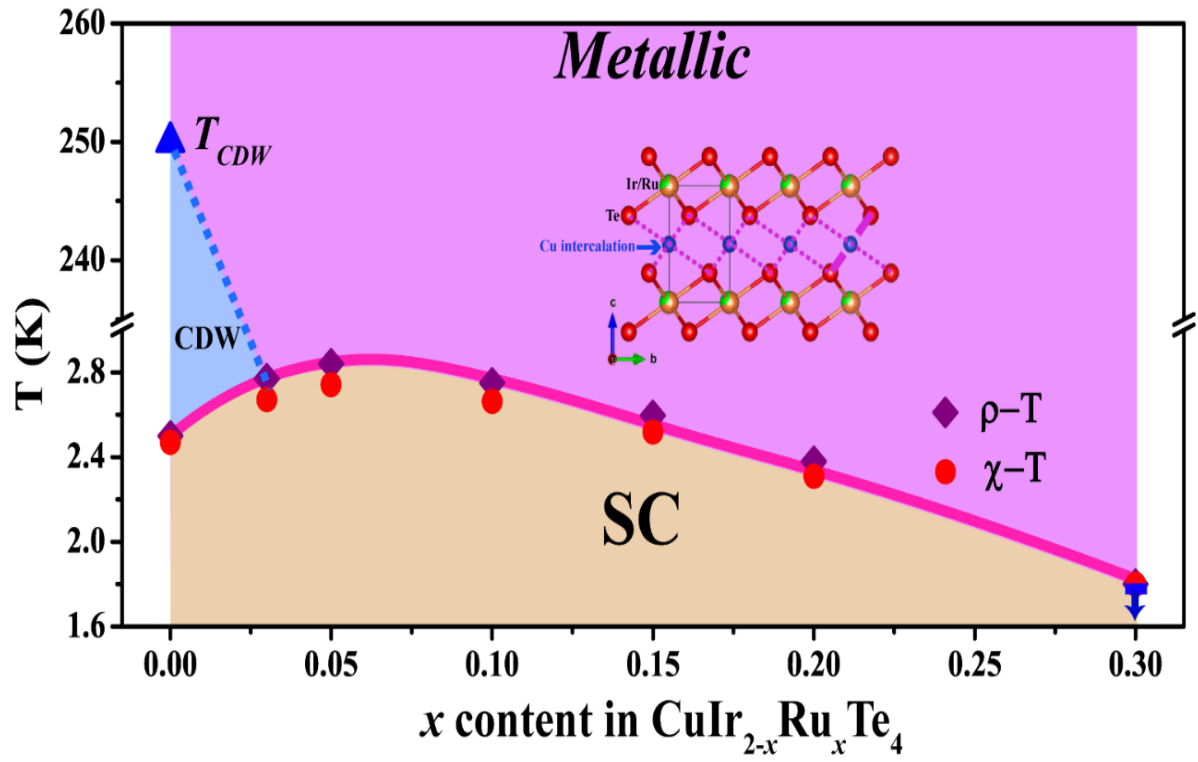


Figure 6. The electronic phase diagram for $\text{CuIr}_{2-x}\text{Ru}_x\text{Te}_4$ ($0.0 \leq x \leq 0.30$).